Nuclear Inst. and Methods in Physics Research, A 957 (2020) 163400

Contents lists available at ScienceDirect

Nuclear Inst. and Methods in Physics Research, A

journal homepage: www.elsevier.com/locate/nima

A novel MLEM stopping criterion for unfolding neutron fluence spectra in radiation therapy

Logan Montgomery [a,*], Anthony Landry [b,c], Georges Al Makdessi [a], Felix Mathew [a], John Kildea [a]

[a] Medical Physics Unit, McGill University, Montreal, QC, H4A3J1, Canada
[b] Prince Edward Island Cancer Treatment Centre, Charlottetown, PE, C1A8T5, Canada
[c] Department of Radiation Oncology, Dalhousie University, Halifax, NS, B3H4RZ, Canada

ARTICLE INFO

Keywords:
MLEM
Neutron
Nested Neutron Spectrometer
Radiotherapy
Unfolding

ABSTRACT

The spectrum of secondary neutrons generated by a medical linear accelerator (linac) during high-energy radiation therapy must be accurately determined in order to assess the carcinogenic risk that these neutrons pose to patients. Neutron spectrometers such as the Nested Neutron Spectrometer (NNS) can be used to measure neutron fluence spectra but the raw measured data must be deconvolved (unfolded) with the detector's response functions. The iterative Maximum-Likelihood Expectation–Maximization (MLEM) algorithm can be used to unfold the raw data, however it lacks an objective stopping criterion and produces an increasingly noisy solution as it iterates. In this work, we describe an objective stopping criterion that terminates MLEM unfolding of secondary neutron spectra in radiation therapy after solution convergence but prior to significant accumulation of noise. We validated the robustness of our stopping criterion by using it to unfold NNS measurements spanning a wide range of neutron fluence rates that were acquired around two linacs. We found that these unfolded spectra demonstrate a high level of agreement with the corresponding ideal unfolded spectra (obtained using Monte Carlo simulated spectra) and are relatively free of noise. Thus, use of our stopping criterion increases confidence in experimentally unfolded neutron spectra and can aid in improving carcinogenic risk estimates for patients receiving radiation therapy.

1. Introduction

The spectrum of secondary neutrons that is produced during high-energy radiation therapy treatments ($\gtrsim 10$ MeV) typically spans thermal energies up to the maximum energy of the primary beam [1–3]. These neutrons deliver unwanted dose to patients, induce activation of materials inside the treatment room, and thus pose a carcinogenic risk to both patients [4,5] and staff [6,7]. Because the carcinogenic risk associated with neutron radiation is believed to vary widely with energy [8,9], accurate risk assessment requires accurate determination of the neutron fluence spectrum.

Neutron spectrometers such as the Bonner sphere spectrometer [10] and the Nested Neutron Spectrometer (NNS) [11] can be used to measure neutron fluence spectra, and both have been used in the context of radiation therapy [12,13]. The raw measurements obtained with these detectors must be deconvolved with the detector's response functions (i.e. unfolded) in order to obtain the spectrum of interest. However, this unfolding problem is typically an under-determined problem having fewer measured data-points than the desired resolution of the spectrum. Thus, mathematically there are an infinite number of spectra that can satisfy a particular set of measurements obtained with one of these neutron spectrometers.

One method to solve an under-determined problem is to use the iterative Maximum-Likelihood Expectation–Maximization (MLEM) algorithm that was first published in 1977 [14]. MLEM is widely used in positron emission tomography (PET) image reconstruction [15] and has been used to unfold neutron fluence spectra by our group [13,16] and others [17]. When convolved with the detector's response functions, the MLEM solution (e.g. a voxelized image when applied to PET, or a fluence spectrum when applied to neutron spectrometry) is that which maximizes the likelihood of producing the measured data. However, it has been shown that the level of random noise in the MLEM solution increases as the number of iterations increases [18] due to (i) the ill-posedness of the problem, (ii) Poisson noise inherent to the measurements, and (iii) imperfections in the modeled detector response [19].

A simple method to reduce noise accumulation in the MLEM solution is to apply a de-noising filter after a fixed number of iterations [20]. Another method is to use the maximum *a priori* approach wherein an additional factor is incorporated into the MLEM formulation that penalizes "roughness" in the estimated solution at each iteration [20]. However, both of these require subjective empirical tuning

* Corresponding author.
E-mail address: logan.montgomery@mail.mcgill.ca (L. Montgomery).

https://doi.org/10.1016/j.nima.2020.163400
Received 18 August 2019; Accepted 4 January 2020
Available online 7 January 2020
0168-9002/

parameters and MLEM must be terminated at an arbitrary and user-dependent number of iterations. One method that does not rely on an empirical tuning parameter, is to introduce a stopping criterion that terminates MLEM when a statistical or heuristic condition has been satisfied.

The objective of this work was to develop an MLEM stopping criterion for unfolding neutron counts-per-second (CPS) data that are measured using the NNS. Specifically, we desired a stopping criterion that terminates unfolding after sufficient convergence to the most likely neutron fluence spectrum but prior to significant accumulation of noise, without requiring subjective user input. Additionally, the stopping criterion must be robust enough to handle the wide range of neutron fluence rates encountered in external beam photon and electron radiation therapy (EBRT; $\sim 10^4$ to 10^6 n·cm^{-2}·s^{-1}). This manuscript describes our method to develop such a stopping criterion and the results of its application.

2. Unfolding NNS measurements using MLEM

Use of the NNS in radiation therapy has been described previously by our group [13,16]. Briefly, the NNS consists of a He-3 proportional counter that is sensitive to thermal neutrons and seven cylindrical high-density polyethylene moderator shells that are assembled in Russian nesting doll fashion. Thermal neutrons undergo neutron capture reactions (n,p) within the He-3 chamber, which are counted to yield a neutron CPS measurement. Neutrons of increasing energy are detected by adding successive moderators around the He-3 chamber such that the entire neutron energy range of interest is sampled.

A set of eight neutron CPS measurements m_i obtained with the NNS must be unfolded with the NNS response functions a_{ij} to yield an estimate of the underlying neutron fluence spectrum n_j. We use the iterative MLEM algorithm to unfold NNS measurements, which is described by:

$$n_j^{k+1} = \frac{n_j^k}{\sum_{i=1}^{I} a_{ij}} \sum_{i=1}^{I} a_{ij} \frac{m_i}{\sum_{b=1}^{J} a_{ib} n_b^k} \tag{1}$$

Here, the index i spans the number of NNS moderator configurations ($I = 8$), j and b span the number of energy bins over which the response functions are defined ($J = 52$), and k is the MLEM iteration index. A new spectrum estimate n_j^{k+1} is generated at each iteration by scaling the previous estimate n_j^k by the normalized ratio of the NNS measurements to the MLEM-reconstructed measurements. For succinctness, we denote the MLEM-reconstructed measurements at each iteration as:

$$q_i^k = \sum_{b=1}^{J} a_{ib} n_b^k \tag{2}$$

A schematic of the unfolding process is shown in Fig. 1. It is important to note that the unfolded spectrum is highly dependent on the initial guess spectrum n_j^0 that is input to the MLEM algorithm. Justification of our choice of the step function shown in Fig. 1 and its application for use in radiation therapy is presented in our previous publication [13].

We cannot directly obtain neutron CPS measurements by operating the He-3 chamber of the NNS as a pulse-counting detector because the high fluence rates encountered in radiation therapy lead to pulse-pileup. Instead, we operate the He-3 chamber in current mode and measure a neutron-induced charge for each moderator configuration using an electrometer. Each charge is first converted to a time-averaged neutron current and subsequently to a neutron CPS measurement using a calibration coefficient that was provided by the vendor and validated by our group [13].

3. The MLEM-STOP method

3.1. Application to PET image reconstruction

The MLEM-STOP method [19] relies on the fact that physical measurements naturally contain Poisson noise such that $m_i = \mu_i + \beta_i$, where μ_i are the mean counts of the distributions from which each corresponding m_i is sampled and β_i are Poisson noise terms. Without a stopping criterion, MLEM infinitely iterates to a spectrum $n_j^{k\to\infty}$ that maximizes the likelihood of reconstructing the noisy m_i. We are actually interested in the ground-truth spectrum $\bar{n}_j$ that maximizes the likelihood of obtaining the noise-free measurements μ_i. To this end, consider the following indicator function that may be evaluated at each MLEM iteration k:

$$\mathcal{J}^k = \frac{\sum_{i=1}^{I} \left(m_i - q_i^k\right)^2}{\sum_{i=1}^{I} q_i^k} \tag{3}$$

After the initial iteration, $\mathcal{J}^k$ has a positive value whose magnitude depends on the guess spectrum n_j^0. As the iterations proceed, the reconstructed measurements converge to the noisy measurements ($q_i^k \to m_i$) such that $\mathcal{J}^k \to 0$. At some intermediate iteration number, the reconstructed measurements may equal the noise-free measurements ($q_i^k = \mu_i$). It is straightforward to show that $\mathcal{J}^k \approx 1$ when this occurs because the expectation value of the mean square deviation (MSD) between a noisy measurement m_i sampled from a Poisson distribution and the mean μ_i is:

$$E\left[\left(m_i - \mu_i\right)^2\right] = \mu_i \tag{4}$$

The basis of MLEM-STOP is thus to set a threshold value, $\mathcal{J}_t = 1$, and terminate unfolding when $\mathcal{J}^k \le \mathcal{J}_t$. At subsequent iterations it is increasingly likely that the noise inherent to each measurement (β_i) is reconstructed rather than the true noise-free measurement (μ_i) from which the noisy measurement was sampled, which leads to noise in the unfolded spectrum.

Ben Bouallègue et al. applied this method to reconstructing images from artificial PET datasets and demonstrated promising results [19]. For each dataset, they compared the MLEM-STOP estimate with (i) a conventional estimate obtained using a fixed number of iterations and (ii) an ideal MLEM estimate. The ideal MLEM estimates were obtained by terminating reconstruction of each dataset when the root mean square error (RMSE) between the reconstructed image and the corresponding ground-truth artificial image was minimized. In terms of noise content and resolution, the MLEM-STOP estimates were better than the conventional (fixed iteration) estimates and very similar to the ideal estimates.

3.2. Application to neutron spectral unfolding

We applied the MLEM-STOP criterion to unfolding neutron CPS measurements obtained with the NNS. However, we found the use of $\mathcal{J}_t = 1$ unsuitable because the rate of MLEM convergence (i.e. the rate at which $m_i/q_i^k \to 1$) is independent of measurement magnitude, but the rate at which $\mathcal{J}^k \to 1$ is not (as explained in the Appendix). As a result, we found that $\mathcal{J}^k > \mathcal{J}_t = 1$ for all k when unfolding high magnitude measurements, which meant that the stopping criterion was never satisfied. Also, when unfolding low magnitude measurements, we found that the stopping criterion was satisfied too early, resulting in spectra that had not sufficiently converged. Thus, we developed a modified MLEM-STOP method that applied well to measurements of varying magnitude that result from neutron fluence rates, Φ, of approximately 10^4 to 10^6 n·cm^{-2}·s^{-1}.

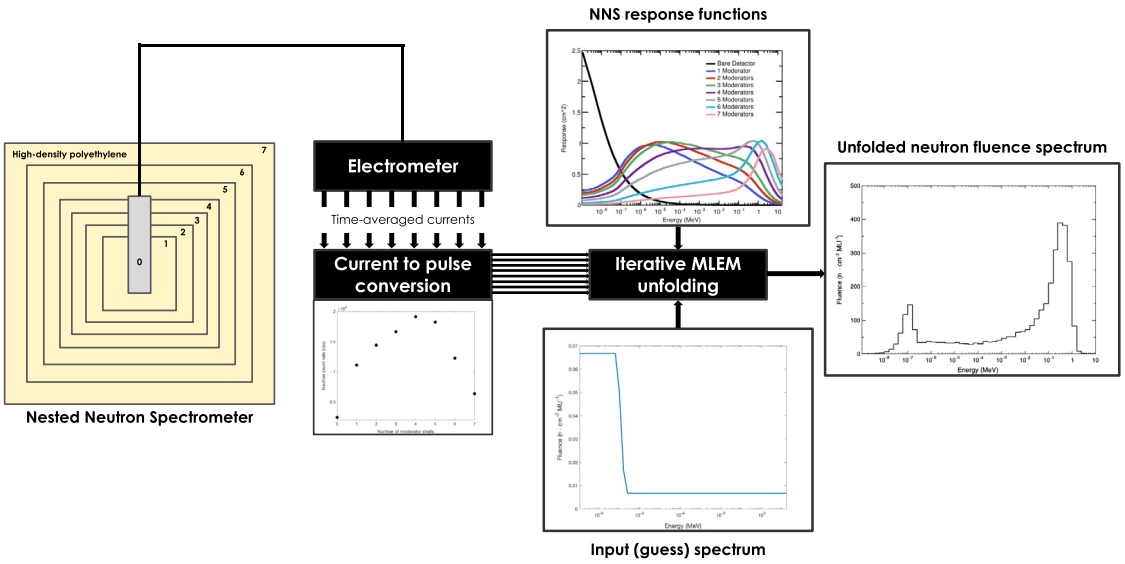

Fig. 1. Schematic of the NNS unfolding process. A time-averaged neutron current is measured for each moderator shell configuration (eight total) and converted to neutron CPS. These neutron CPS are input into a custom MLEM algorithm along with the NNS response functions and a guess spectrum. The algorithm iterates until terminated, yielding an estimate of the neutron fluence spectrum. (For interpretation of the references to color in this figure legend, the reader is referred to the web version of this article.)

4. A modified MLEM-STOP method

This section explores the core idea of our modified MLEM-STOP method; that there exists an optimal average measurement magnitude $\bar{m}_{\text{ideal}}$ (and corresponding neutron fluence) at which the $\mathcal{J}_t = 1$ stopping criterion best applies. We describe how we determined $\bar{m}_{\text{ideal}}$ using ideal unfolded spectra and then capitalized on the linearity of MLEM to establish a new stopping criterion that may be applied when unfolding measurements spanning a broad range of magnitudes.

4.1. Ideal unfolded spectra

As described by Ben Bouallègue et al. [19], the ideal unfolded estimate $n_j^{k_{\text{ideal}}}$ of the ground-truth spectrum $\bar{n}_j$ is determined by calculating the root mean square error (RMSE) between $\bar{n}_j$ and the MLEM estimate n_j^k at each iteration:

$$\text{RMSE}^k = \sqrt{\frac{\sum_{j=1}^{J}\left(\bar{n}_j - n_j^k\right)^2}{J}} \tag{5}$$

The ideal unfolded spectrum $n_j^{k_{\text{ideal}}}$ is obtained when the RMSE is minimized and represents an ideal compromise between solution convergence and noise. Note that RMSE can only be calculated if the ground-truth is known and thus minimization of RMSE cannot be used experimentally as a stopping criterion.

In this work, we required $n_j^{k_{\text{ideal}}}$ for multiple spectra spanning a wide range of neutron fluence in order to determine the optimal measurement magnitude $\bar{m}_{\text{ideal}}$ at which the $\mathcal{J}_t = 1$ criterion best applies. As described in our previous publication on validating the NNS for use in radiation therapy [13], we simulated and experimentally measured the photoneutron fluence spectra produced by the 18 MV beam of a Varian Clinac 21EX at four locations in the treatment room for which the neutron fluences varied significantly. These locations are shown in Fig. 2(a). The simulations were performed using the Monte Carlo modeling package MCNP6 [21] with validated in-house models of the linac (including accelerator components and shielding) and the treatment room. In the present work, we assumed that each simulated spectrum was equivalent to the ground-truth spectrum $\bar{n}_j$ at the corresponding location. The experimental $n_j^{k_{\text{ideal}}}$ was then determined for each of the four NNS measurement sets by calculating the RMSE between the simulated ground-truth and the reconstructed experimental spectrum at each MLEM iteration (using Eq. (5)), and terminating when minimized.

4.2. A new stopping criterion

For each of the four datasets for which we determined $n_j^{k_{\text{ideal}}}$, we calculated the mean deviation (MD) between the experimental measurements and their corresponding reconstructed measurements at the ideal number of iterations ($q_i^{k_{\text{ideal}}}$):

$$\text{MD} = \frac{\sum_{i=1}^{I}\left|m_i - q_i^{k_{\text{ideal}}}\right|}{I} \tag{6}$$

We plotted the MD for each dataset as a function of the average measurement magnitude (i.e. $\bar{m} = \sum_{i=1}^{I} m_i/I$), as shown in Fig. 3. As previously stated, the rate of MLEM convergence is independent of measurement magnitude and consequently the MD between measurements and their reconstructions is linear with respect to measurement magnitude. Thus, a linear least-squares regression through the origin was performed on these four data points, the result of which is shown as the solid line in Fig. 3. This fitted line represents the level of MLEM convergence attained at the ideal number of iterations as a function of $\bar{m}$. Note that we forced a zero y-intercept because otherwise the regression produced a negative intercept that erroneously implies a negative MD for data with low $\bar{m}$.

This result was compared with the principle assumption of the MLEM-STOP method, namely that $q_i^k \to \mu_i$ at some k. The expectation value of the MD between the mean of a Poisson distribution and values sampled from the distribution is shown as the dotted line in Fig. 3 and is calculated by [22]:

$$\text{MD} = \frac{2e^{-\bar{m}}\bar{m}^{\bar{m}+1}}{\bar{m}!} \tag{7}$$

The point where the two curves in Fig. 3 overlap is the optimal magnitude ($\bar{m}_{\text{ideal}} \approx 30\,000$ CPS) at which the ideal level of MLEM convergence is aligned with the assumption of MLEM-STOP. This leads to three possible scenarios:

1. If $\bar{m} = \bar{m}_{\text{ideal}}$, MLEM converges to the ideal unfolded spectrum $n_j^{k_{\text{ideal}}}$ around when $\mathcal{J}^k = \mathcal{J}_t = 1$.
2. If $\bar{m} > \bar{m}_{\text{ideal}}$, MLEM converges to $n_j^{k_{\text{ideal}}}$ at some point when $\mathcal{J}^k > \mathcal{J}_t = 1$ because the ideal experimental MD is greater than the theoretical expectation.
3. If $\bar{m} < \bar{m}_{\text{ideal}}$, MLEM converges to $n_j^{k_{\text{ideal}}}$ at some point when $\mathcal{J}^k < \mathcal{J}_t = 1$ because the ideal experimental MD is less than the theoretical expectation.

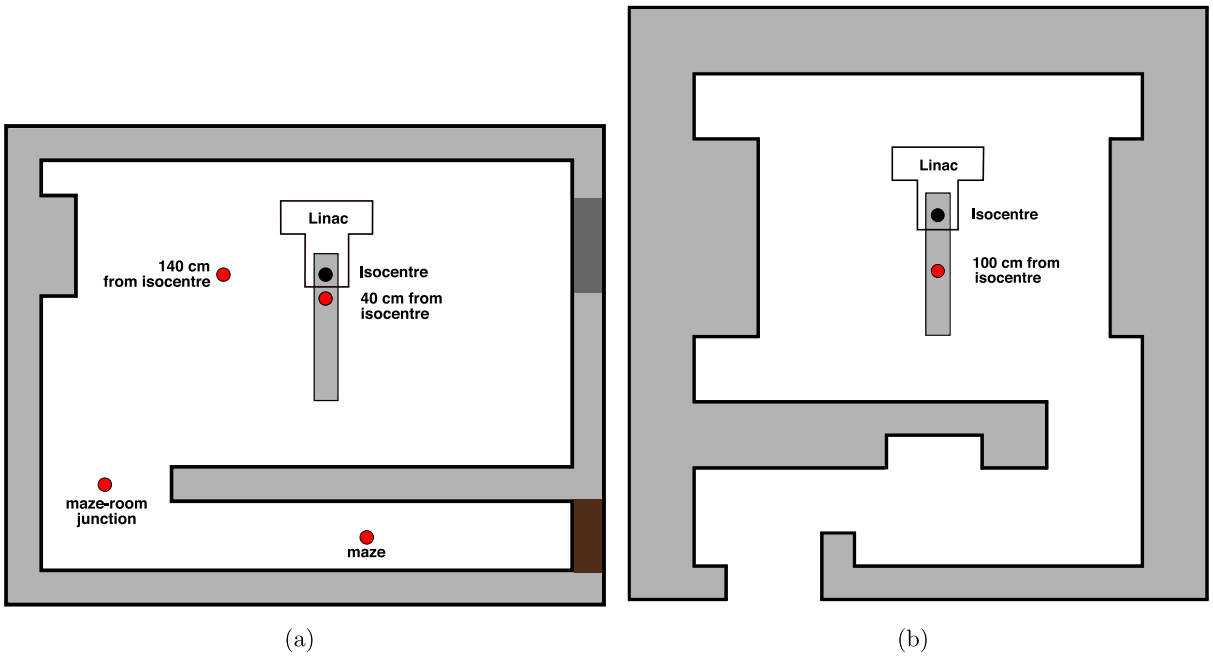

Fig. 2. Schematics of the radiation therapy treatment rooms in which neutron spectral measurements were made. Measurement locations are indicated in red. Figures not to scale. (a) Treatment room housing the Varian Clinac 21EX with a door. Measurements were used to develop and validate our novel stopping criterion. (b) Doorless treatment room housing the Varian Truebeam. Measurements were used to further test our stopping criterion. (For interpretation of the references to color in this figure legend, the reader is referred to the web version of this article.)

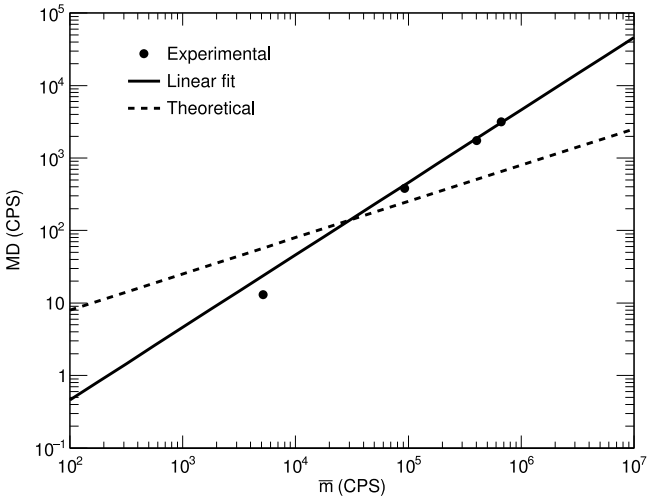

Fig. 3. Comparison of the mean deviation (MD) between NNS measurements and MLEM reconstructed measurements (data points), and the expectation value of the MD between the mean and sampled values of a Poisson distribution (dashed line), as a function of mean neutron CPS. The solid line represents a linear fit through the origin to the experimental MLEM data.

These scenarios clarify and quantify our earlier findings that MLEM-STOP does not apply well to high magnitude measurements (never reaches $\mathcal{J}^k = \mathcal{J}_t = 1$) nor to low magnitude measurements (insufficient convergence when $\mathcal{J}^k = \mathcal{J}_t = 1$).

Fortunately, since the rate of MLEM convergence is independent of $\bar{m}$, one can simply scale any set of measurements such that $\bar{m} = \bar{m}_{\text{ideal}}$ by multiplying by $\bar{m}_{\text{ideal}}/\bar{m}$. These scaled measurements can then be unfolded using MLEM-STOP, which is terminated when $\mathcal{J}^k \leq \mathcal{J}_t = 1$. Following this approach, the final unfolded spectrum must be scaled back by the inverse ratio, $\bar{m}/\bar{m}_{\text{ideal}}$. An alternative approach that is simpler than scaling the measurements is to specify a new threshold value for each unique dataset:

$$\mathcal{J}_t = \frac{\bar{m}}{\bar{m}_{\text{ideal}}} \tag{8}$$

and terminate when $\mathcal{J}^k \leq \mathcal{J}_t = \bar{m}/\bar{m}_{\text{ideal}}$. This latter approach is more succinctly stated as a stopping criterion and was adopted as our modified MLEM-STOP criterion.

4.3. Uncertainty calculations

A statistical uncertainty in each neutron fluence spectrum obtained using the modified MLEM-STOP method was estimated using a random sampling process that was adapted from the method described in our previous publication [13]. All eight measurements m_i in an NNS dataset were set as the mean of a Poisson distribution and each distribution was subsequently sampled 100 times to yield 100 pseudo-measurement sets. All of the pseudo-measurement sets were then unfolded using the modified MLEM-STOP method. The root mean square difference between the experimental unfolded spectrum and the 100 unfolded pseudo-spectra was then set as the spectrum uncertainty.

5. Results

5.1. Validation: comparison with ideal unfolded spectra

To validate our modified MLEM-STOP method, we applied it to all four NNS datasets for which $n_j^{k_{\text{ideal}}}$ and $\bar{n}_j$ were known (i.e. the measurements made at the locations indicated in Fig. 2(a)). The resulting MLEM-STOP spectra are plotted alongside $n_j^{k_{\text{ideal}}}$ and $\bar{n}_j$ in Fig. 4. The ideal number of iterations (k_{ideal}) and the number of iterations determined for use in MLEM-STOP, denoted k_{STOP}, are provided in Table 1.

5.2. Testing: comparison with a conventional unfolding approach

To further test our modified MLEM-STOP criterion, we applied it to the unfolding of three NNS datasets for which $\bar{n}_j$ and thus $n_j^{k_{\text{ideal}}}$ were unknown. These datasets comprised NNS measurements at 100 cm

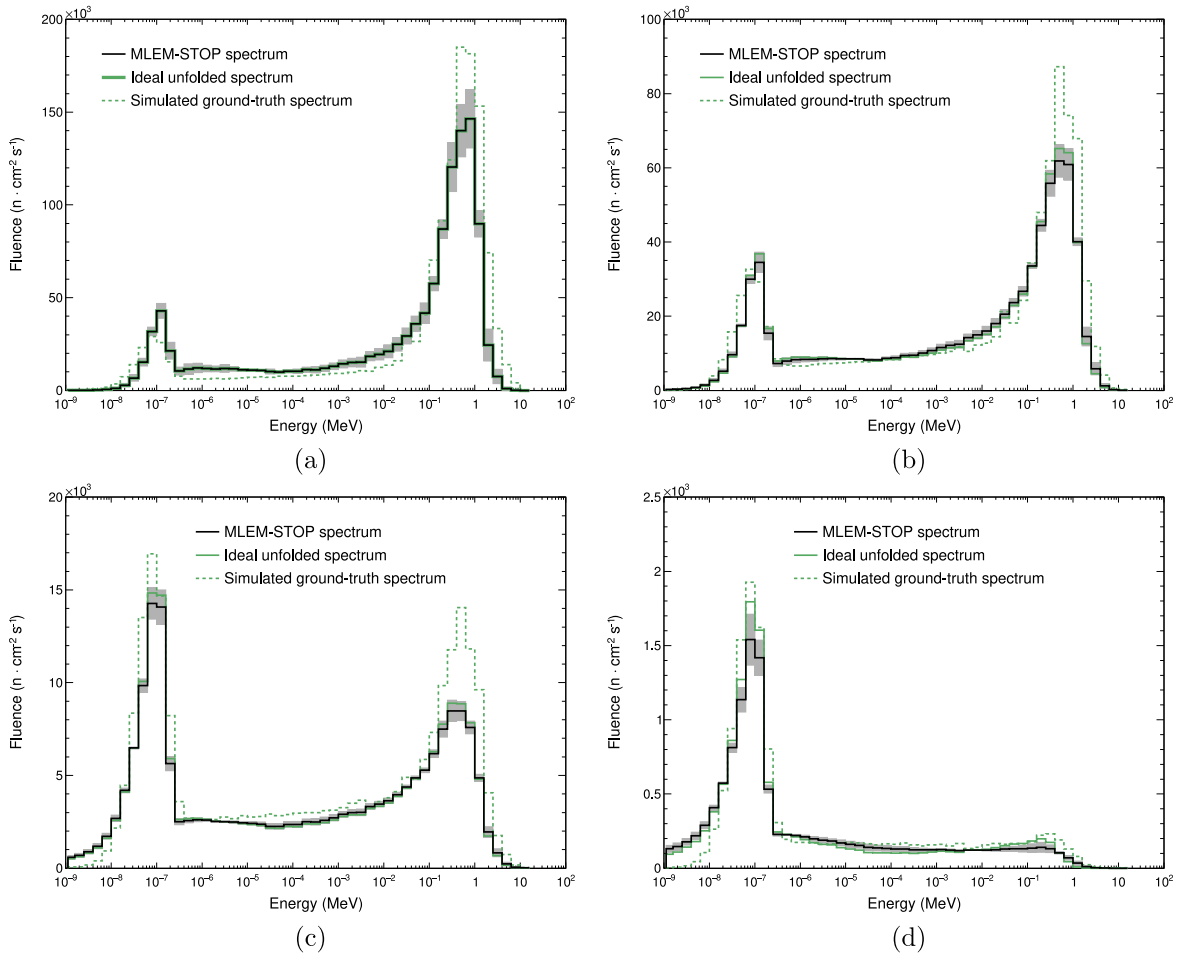

Fig. 4. Comparison of neutron fluence spectra obtained by unfolding NNS measurements using our modified MLEM-STOP method (solid black) with corresponding ideal unfolded spectra (solid green) and Monte Carlo simulated spectra that were assumed to be equivalent to the ground-truth (dashed green). Spectra were obtained using the 18 MV beam of a Varian Clinac at four locations around the treatment room; (a) at 40 cm from isocentre, (b) at 140 cm from isocentre, (c) at the maze-room junction, and (d) in the maze. (For interpretation of the references to color in this figure legend, the reader is referred to the web version of this article.)

Table 1
The number of iterations, k_{STOP}, required to satisfy our modified MLEM-STOP criterion for all experimental NNS datasets considered in this work. Datasets are grouped according to their purpose and within each group are sorted in order of decreasing neutron fluence rate Φ. The number of iterations, k_{ideal}, corresponding to the ideal unfolded spectra are provided for the 18 MV datasets used to develop and validate our method.

Purpose	Beam energy	Location	Φ $(n \cdot cm^{-2} \cdot s^{-1})$	k_{ideal}	k_{STOP}
Validation	18 MV	40 cm from isocentre	$(1.23 \pm 0.02) \times 10^6$	3687	3699
	18 MV	140 cm from isocentre	$(7.64 \pm 0.07) \times 10^5$	2742	2113
	18 MV	maze-room junction	$(1.90 \pm 0.01) \times 10^5$	2059	1674
	18 MV	maze	$(1.22 \pm 0.01) \times 10^4$	5632	1182
Testing	15 MV	100 cm from isocentre	$(2.56 \pm 0.03) \times 10^5$	N/A	3873
	10 MV	100 cm from isocentre	$(2.18 \pm 0.03) \times 10^4$	N/A	3879
	16 MeV	100 cm from isocentre	$(1.36 \pm 0.01) \times 10^4$	N/A	2805

from isocentre along the treatment couch of a Varian Truebeam linac, as indicated in Fig. 2(b). Measurements for the 15 MV and 10 MV photon beams as well as the 16 MeV electron beam were obtained. The unfolded spectra are shown in Fig. 5 and the corresponding k_{STOP} values are provided in Table 1.

In the absence of ground-truth, we compared each MLEM-STOP spectrum with two spectra obtained by terminating unfolding at fixed iteration numbers that serve as empirical upper and lower limits, between which unfolding should usually be terminated. The upper limit was set as $k_{upper} = 15000$ because we observed that significant noise, in the form of adjacent bins of alternating high and low magnitude, is typically visible in the intermediate energy region ($\sim$ 1 eV to 10 keV) at this number of iterations and above. The lower limit was set as $k_{lower} = 1000$ because with fewer iterations the fast and thermal peaks are typically poorly-defined, which indicates insufficient convergence. These peaks are known to be well-defined for secondary neutron spectra in photon and electron EBRT, as widely reported in the literature and observed in our own Monte Carlo simulated spectra [1,2,13]. The spectra obtained at these upper and lower limits are shown alongside the MLEM-STOP spectra in Fig. 5. Note that the Poisson sampling approach described in Section 4.3 was also used to estimate uncertainties for the upper and lower limit spectra with the exception that the corresponding fixed number of iterations was used as the stopping criterion for each set of pseudo-measurements (instead of MLEM-STOP).

To demonstrate the dosimetric impact of the spectral differences shown in Fig. 5, the neutron ambient dose equivalent rate, $\dot{H}^*(10)$, was calculated for each MLEM-STOP spectrum as well as for the conventional upper and lower limits. $\dot{H}^*(10)$ was calculated by multiplying the

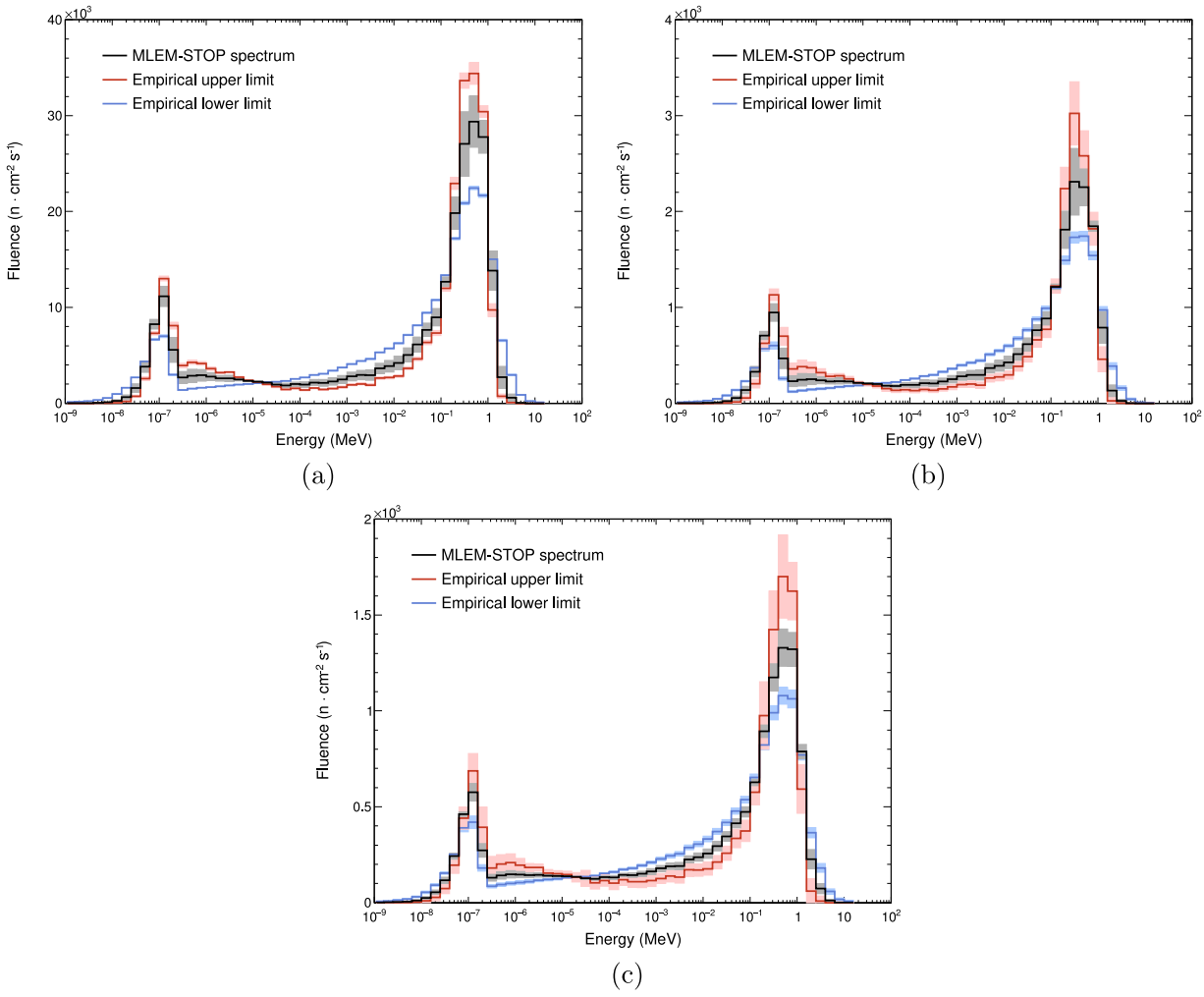

Fig. 5. Comparison of neutron fluence spectra obtained by unfolding NNS measurements using our modified MLEM-STOP method (black) with unfolded spectra using fixed iteration numbers corresponding to empirical upper (red) and lower (blue) limits. An upper limit of k_{upper} = 15000 iterations and a lower limit of k_{lower} = 1000 iterations were used. Spectra were measured at 100 cm from isocentre along the treatment couch for two photon beams and one electron beam of a Varian Truebeam linac: (a) 15 MV, (b) 10 MV, and (c) 16 MeV. (For interpretation of the references to color in this figure legend, the reader is referred to the web version of this article.)

Table 2
Neutron ambient dose equivalent rates, $\dot{H}^*(10)$, associated with unfolded neutron fluence spectra obtained using MLEM-STOP versus empirical upper and lower iteration limits.

Beam energy	$\dot{H}^*(10)$ (mSv · hr^{-1})		
	Empirical lower limit	MLEM-STOP	Empirical upper limit
15 MV	124.7 ± 0.7	131 ± 2	135 ± 1
10 MV	9.20 ± 0.07	9.7 ± 0.2	10.1 ± 0.1
16 MeV	6.31 ± 0.03	6.6 ± 0.1	6.84 ± 0.07

measured fluence rate in each energy bin by the appropriate neutron fluence-to-dose conversion coefficient provided in ICRP-74 [23] and by summing over all bins. The resulting $\dot{H}^*(10)$ values are provided in Table 2. Uncertainties were set as the root mean square deviation between the experimental $\dot{H}^*(10)$ value and the pseudo-$\dot{H}^*(10)$ values calculated for all 100 pseudo-spectra that were generated for the corresponding spectral uncertainty calculations.

6. Discussion

Our modified MLEM-STOP method utilizes a statistical stopping criterion that terminates iterative MLEM unfolding of secondary neutron fluence spectra in EBRT without subjective user input. The spectra obtained with this method demonstrate a high level of agreement with the corresponding ideal unfolded spectra (obtained through comparison with Monte Carlo simulated spectra), as shown in Fig. 4. This serves as validation of our method for neutron fluence spectra ranging from $\Phi \approx 10^4$ to 10^6 n·cm^{-2}·s^{-1}. It is important to note that the experimental unfolded spectra (MLEM-STOP and ideal) do not agree completely with the simulated spectra. This could be due to inaccuracies in the Monte Carlo models, limitations of the resolution of NNS measurements, and the ill-posed nature of the unfolding problem. However, this does not undermine our finding that MLEM-STOP is able to generate spectra that are almost entirely within uncertainty of the ideal unfolded spectra.

The modified MLEM-STOP approach was also applied to NNS measurements for which the ground-truth spectra were unknown; the results of which are shown in Fig. 5. These spectra appear reasonable because of the well-defined fast and thermal peaks (demonstrating sufficient convergence) as well as the limited presence of visible noise in the intermediate energy region. We do not have simulated ground-truth spectra to compare with because the specifications of the beam shaping assembly of the Varian Truebeam linac is not disclosed by the vendor, and we are thus unable to model it for Monte Carlo simulations. However, through comparison with the empirical upper and lower limits, the MLEM-STOP spectra appear to satisfy our goal to produce spectra that have sufficiently converged with minimal noise.

The effect of the spectral shape (and thus iteration number) on the dosimetric quantity of interest, $\dot{H}^*(10)$, is elucidated in Table 2. For all three datasets, the ambient dose equivalent rate associated

Table A.1
Comparison between the ratio of measurements to MLEM-reconstructed measurements at $k = 2784$ iterations for an arbitrary NNS measurement set m_i and an artificial measurement set M_i such that $M_i = 10m_i$.

# moderators	m_i (CPS)	q_i^k (CPS)	$\frac{m_i}{q_i^k}$	M_i (CPS)	Q_i^k (CPS)	$\frac{M_i}{Q_i^k}$
0	2129	2132	0.9988	21290	21320	0.9988
1	10340	10265	1.0073	103400	102650	1.0073
2	13207	13228	0.9984	132070	132280	0.9984
3	15457	15560	0.9934	154570	155600	0.9934
4	17635	17721	0.9951	176350	177210	0.9951
5	17035	16881	1.0091	170350	168810	1.0091
6	11476	11431	1.0039	114760	114310	1.0039
7	6156	6217	0.9903	61560	62170	0.9903

with the MLEM-STOP spectrum is significantly different from both the empirical upper and lower limits. These differences arise from the tendency of the dominant peak (in these cases, the fast peak) to increase in magnitude as MLEM iterates. This finding, coupled with the fact that the fluence-to-dose conversion coefficients are peaked around 1 MeV [23], results in the observed dosimetric discrepancies. Although there are no ground-truth $\dot{H}^*(10)$ values to compare with, the MLEM-STOP estimates are a good compromise between the upper and lower limits.

As shown in Table 1, the fluence rates of the spectra with no known ground-truth are within the range spanned by the 18 MV spectra with known ground-truth. We anticipate that the modified MLEM-STOP method is applicable for any set of measurements wherein each measurement m_i is governed by Poisson statistics because MLEM behaves linearly with measurement magnitude. Regarding the unfolding of measurements acquired using the NNS specifically, there may be experimental limitations at low fluence rates due to insufficient signal relative to the noise and at high fluence rates due to loss of linearity of the He-3 chamber.

Finally, the dynamic threshold, $\mathcal{J}_t$, of our modified MLEM-STOP method is calculated using $\bar{m}_{\text{ideal}}$ as shown in Eq. (8) and thus the MLEM-STOP spectra are sensitive to the fitting procedure used to determine $\bar{m}_{\text{ideal}}$. Furthermore, we believe our method may be applied generally to other "classes" of spectra having significantly different shapes. However, if a different guess spectrum is required, or if the level of convergence associated with ideal unfolded spectra differs significantly from the fitted curve of Fig. 3, then a new calibration should be performed to determine $\bar{m}_{\text{ideal}}$. With knowledge of a few ground-truth spectra, the procedure of Section 4.2 could then be used to determine $\bar{m}_{\text{ideal}}$ for the "class" of spectra under consideration.

Our software for unfolding and plotting neutron spectra, including our modified MLEM-STOP algorithm, is provided as open-source software on Github [24].

7. Conclusions

We have developed a statistical stopping criterion to terminate iterative MLEM unfolding of secondary neutron spectra in external beam photon and electron radiation therapy as measured using the Nested Neutron Spectrometer. This stopping criterion is based on the MLEM-STOP methodology published for PET image reconstruction by Ben Bouallègue et al. [19], and is designed to terminate unfolding after sufficient solution convergence but prior to significant accumulation of noise. Modifications to the published method were required to accommodate the wide range of neutron fluence rates encountered in radiation therapy. Our modified approach uses a dynamic threshold value that is calculated for each unique set of measurements. We obtained good agreement between the spectra unfolded using our modified MLEM-STOP method and the ideal unfolded spectra obtained using knowledge of the underlying ground-truth spectra. When applied to datasets with unknown ground-truth, we found that the MLEM-STOP spectra qualitatively met the theoretical goals of the method. This method should be generally applicable to measurements of any magnitude but may require a unique calibration using known ground-truth for spectra having distinct spectral shapes and alternative guess input spectra.

Acknowledgments

This work was supported by the Natural Sciences and Engineering Research Council of Canada (NSERC) (Alexander Graham Bell Canada Graduate Scholarship-Doctoral: L. Montgomery, Discovery Grant: J. Kildea). Partial support for this research was provided by the CREATE Medical Physics Research Training Network grant of the Natural Sciences and Engineering Research Council of Canada (Grant number: 432290) and by the Canadian Nuclear Safety Commission (CNSC). A Nested Neutron Spectrometer used in this investigation was generously provided on loan from the CNSC. Logistical support provided by the Prince Edward Island Cancer Treatment Centre was invaluable for this work. Insightful advice and discussions provided by Jacques Dubeau (Detec Inc.) and Angel Licea (CNSC) are gratefully appreciated.

Appendix. Incompatible convergence rates

This appendix demonstrates why the rate at which ${}^{m_i}/_{q_i^k} \to 1$ is independent of measurement magnitude but the rate at which $\mathcal{J}^k \to 1$ is not. Consider MLEM unfolding of an arbitrary set of NNS measurements, m_i, provided in Table A.1. The reconstructed measurements, q_i^k, after $k = 2784$ iterations of MLEM are also provided in Table A.1. When these data are used to calculate $\mathcal{J}^k$ via Eq. (3), a result of $\mathcal{J}^k = 1$ is obtained.

Now consider another set of eight NNS measurements, M_i such that $M_i = 10m_i$. When these are unfolded using the same number of iterations ($k = 2784$) the resulting MLEM-reconstructed measurements, Q_i^k, are equal to $10 \times q_i^k$ as shown in Table A.1. Thus, the ratios ${}^{m_i}/_{q_i^k}$ and ${}^{M_i}/_{Q_i^k}$ are equal, which indicates that the rate of MLEM convergence is independent of measurement magnitude. However, when M_i and Q_i^k are used to calculate $\mathcal{J}^k$ at $k = 2784$, a result of $\mathcal{J}^k = 5.7$ is obtained. This occurs because calculation of $\mathcal{J}^k$ involves calculating mean square differences between two values, which increases with the magnitude of the values even if their relative values are constant.

References

[1] R.M. Howell, S.F. Kry, E. Burgett, N.E. Hertel, D.S. Followill, Secondary neutron spectra from modern Varian, Siemens, and Elekta linacs with multileaf collimators, Med. Phys. 36 (9) (2009) 4027–4038, http://dx.doi.org/10.1118/1.3159300.

[2] H. Vega-Carrillo, L. Pérez-Landeros, Electroneutrons around a 12 MV LINAC, in: 13 International Symposium: Sociedad Mexicana de Irradiacion y Dosimetria, 2012, pp. 26–29.

[3] R.M. Howell, E.A. Burgett, Secondary neutron spectrum from 250 MeV passively scattered proton therapy: Measurement with an extended range Bonner sphere system, Med. Phys. 41 (2014) 092104, http://dx.doi.org/10.1118/1.4892929.

[4] S.F. Kry, B. Bednarz, R.M. Howell, L. Dauer, D. Followill, E. Klein, H. Paganetti, B. Wang, C.-S. Wuu, X.G. Xu, AAPM TG 158: Measurement and calculation of doses outside the treated volume from external-beam radiation therapy, Med. Phys. 44 (10) (2017) e391–e429, http://dx.doi.org/10.1002/mp.12462.

[5] W.D. Newhauser, M. Durante, Assessing the risk of second malignancies after modern radiotherapy, Nature Rev. Cancer 11 (6) (2011) 438–448, http://dx.doi.org/10.1038/nrc3069.

[6] Y.Z. Wang, M.D.C. Evans, E.B. Podgorsak, Characteristics of induced activity from medical linear accelerators, Med. Phys. 32 (9) (2005) 2899–2910, http://dx.doi.org/10.1118/1.2001767.

[7] J. Rawlinson, M.K. Islam, D.M. Galbraith, Dose to radiation therapists from activation at high-energy accelerators used for conventional and intensity-modulated radiation therapy, Med. Phys. 29 (4) (2002) 598–608, http://dx.doi.org/10.1118/1.1463063.

[8] ICRP, The 2007 Recommendations of the International Commission on Radiological Protection. ICRP Publication 103, Ann. ICRP 37 (2–4) (2007).

[9] G. Baiocco, S. Barbieri, G. Babini, J. Morini, D. Alloni, W. Friedland, P. Kundrát, E. Schmitt, M. Puchalska, L. Sihver, A. Ottolenghi, The origin of neutron biological effectiveness as a function of energy, Sci. Rep. 6 (2016) 34033, http://dx.doi.org/10.1038/srep34033.

[10] R.L. Bramblett, R.I. Ewing, T.W. Bonner, A new type of neutron spectrometer, Nucl. Instrum. Methods 9 (1) (1960) 1–12, http://dx.doi.org/10.1016/0029-554X(60)90043-4.

[11] J. Dubeau, S.S. Hakmana Witharana, J. Atanackovic, A. Yonkeu, J.P. Archambault, A neutron spectrometer using nested moderators, Radiat. Prot. Dosim. 150 (2) (2012) 217–222, http://dx.doi.org/10.1093/rpd/ncr381.

[12] R.M. Howell, N.E. Hertel, Z. Wang, J. Hutchinson, G.D. Fullerton, Calculation of effective dose from measurements of secondary neutron spectra and scattered photon dose from dynamic MLC IMRT for 6 MV, 15 MV, and 18 MV beam energies, Med. Phys. 33 (2) (2006) 360–368, http://dx.doi.org/10.1118/1.2140119.

[13] R. Maglieri, A. Licea, M. Evans, J. Seuntjens, J. Kildea, Measuring neutron spectra in radiotherapy using the nested neutron spectrometer, Med. Phys. 42 (11) (2015) 6162–6169, http://dx.doi.org/10.1118/1.4931963.

[14] A.P. Dempster, N.M. Laird, D.B. Rubin, Maximum likelihood from incomplete data via the EM algorithm, J. R. Stat. Soc. Ser. B Stat. Methodol. 39 (1) (1977) 1–38, http://dx.doi.org/10.1111/j.2517-6161.1977.tb01600.x.

[15] L.A. Shepp, Y. Vardi, Maximum likelihood reconstruction for emission tomography, IEEE Trans. Med. Imaging 1 (2) (1982) 113–122, http://dx.doi.org/10.1109/TMI.1982.4307558.

[16] L. Montgomery, M. Evans, L. Liang, R. Maglieri, J. Kildea, The effect of the flattening filter on photoneutron production at 10 MV in the Varian TrueBeam linear accelerator, Med. Phys. 45 (10) (2018) 4711–4719, http://dx.doi.org/10.1002/mp.13148.

[17] B. Pehlivanovic, S. Avdic, P. Marinkovic, S.A. Pozzi, M. Flaska, Comparison of unfolding approaches for monoenergetic and continuous fast-neutron energy spectra, Radiat. Meas. 49 (2013) 109–114, http://dx.doi.org/10.1016/j.radmeas.2012.12.008.

[18] D.L. Synder, M.I. Miller, L.J. Thomas, D.G. Politte, Noise and edge artifacts in maximum-likelihood reconstructions for emission tomography, IEEE Trans. Med. Imaging 6 (3) (1987) 228–238, http://dx.doi.org/10.1109/TMI.1987.4307831.

[19] F. Ben Bouallègue, J.F. Crouzet, D. Mariano-Goulart, A heuristic statistical stopping rule for iterative reconstruction in emission tomography, Ann. Nuclear Med. 27 (1) (2013) 84–95, http://dx.doi.org/10.1007/s12149-012-0657-5.

[20] E. Garduño, G.T. Herman, Superiorization of the ML-EM algorithm, IEEE Trans. Nucl. Sci. 61 (1) (2014) 162–172, http://dx.doi.org/10.1109/TNS.2013.2283529.

[21] T. Goorley, M. James, T. Booth, F. Brown, J. Bull, L.J. Cox, J. Durkee, J. Elson, M. Fensin, R.A. Forster, J. Hendricks, H.G. Hughes, R. Johns, B. Kiedrowski, R. Martz, S. Mashnik, G. McKinney, D. Pelowitz, R. Prael, J. Sweezy, L. Waters, T. Wilcox, T. Zukaitis, Initial MCNP6 release overview, Nucl. Technol. 180 (3) (2012) 298–315, http://dx.doi.org/10.13182/NT11-135.

[22] E.L. Crow, The mean deviation of the Poisson distribution, Biometrika 45 (3–4) (1958) 556–562, http://dx.doi.org/10.1093/biomet/45.3-4.556.

[23] ICRP, Conversion coefficients for use in radiological protection against external radiation. ICRP Publication 74, Ann. ICRP 26 (3–4) (1996).

[24] L. Montgomery, G. Al Makdessi, R. Maglieri, F. Mathew, J. Kildea, Neutron Spectrometry, Github repository (2020) http://dx.doi.org/10.5281/zenodo.3610493.